International Journal of Thermal Sciences 204 (2024) 109201

Contents lists available at ScienceDirect

International Journal of Thermal Sciences

journal homepage: www.elsevier.com/locate/ijts

# Thermal protection of the nuclear rocket engine nozzle based on regenerative cooling method

Si Yang [a], Hangbin Zhao [b,c,*], Nailiang Zhuang [a,c], Xiaobin Tang [a,c,**]

[a] Department of Nuclear Science and Technology, Nanjing University of Aeronautics and Astronautics, Nanjing 211106, China
[b] College of Astronautics, Nanjing University of Aeronautics and Astronautics, Nanjing, 211106, China
[c] Key Laboratory of Nuclear Technology Application and Radiation Protection in Astronautics, Ministry of Industry and Information Technology, Nanjing, 211106, China

ARTICLE INFO

*Keywords:*
Thermal protection
Nuclear rocket
Regenerative cooling
Composite structure
Heat convection

ABSTRACT

In the design of the nuclear rocket engine nozzles, the heat in the throat area of nozzles is so intense that the temperature may exceed the endurance of existing materials. Regenerative cooling technology is a widely employed method for effectively cooling the nozzle. The influences of a strategy involving the arrangement of ribs in the regenerative cooling channel are investigated. The flow and heat transfer characteristics in the regenerative cooling channels with three different types of ribs are compared and analyzed. In accordance with the computational results, two composite structures are proposed. Moreover, the flow and heat transfer characteristics in the bending channel with these two composite structures are calculated and analyzed. The results show that the straight and streamlined ribs can reduce the maximum temperature only when the height is lower than 1 mm. The side rib can reduce the temperature near the rib. For the composite rib, when the distance between the side rib and bottom rib is ranging from 3 cm to 5 cm, the appearance of the high temperature zone, which is located near the bottom rib can be prevented. Moreover, in the bending channel, the straight composite rib can considerably reduce the maximum temperature in the throat area by 96 K. However, the streamlined composite rib can only reduce the wall temperature near the rib.

## 1. Introduction

Nuclear energy is one of the most promising space heat and energy source owning to its advantages of high-power density and stability [1]. Diverse space applications of nuclear energy have been developed or researched, such as space nuclear reactors [2], radioisotope thermoelectric generators and nuclear rocket engines [3]. Compared with chemical rocket engines, nuclear rocket engines have numerous outstanding advantages, including large thrust, long life, and high specific impulse [4]. Given this good performance, nuclear rocket engines can fulfill the demand of power in future large-scale deep space exploration and manned Mars exploration [5]. However, in the existing design, the throat area of the nozzle, suffers from high temperature. The extreme heat flux may lead to the rupture of the nozzle wall. Furthermore, the reduction of the engine thrust and the destruction of the engine may not be avoidable [6].

The regenerative cooling method is the most prevalent design of thermal protection for chemical rockets [7]. Offering the strongest cooling effect, this method can ensure that the rocket engine nozzle is protected from the high heat flux. However, in the nuclear rocket engine designs, the supercritical hydrogen flows into the regenerative cooling channel around the nozzle. As the hydrogen flows, it absorbs the heat from the nozzle wall and then enters the core [8]. Hence, the coolant pressure in the nuclear thermal rocket surpasses that of chemical rockets, and the heat flux in the nozzle throat area is significantly higher [9]. Li [10] constructed a three-dimensional nozzle model. In this model, the regenerative cooling structure is designed as a traditional rectangular channel. Therefore, the regenerative cooling channels are uniformly distributed circumferentially outside the nozzle wall. The results showed that, near the throat area of the nozzle, the temperature slightly exceeds the upper limit. Consequently, enhancing the nozzle thermal protection becomes increasingly apparent.

Research on optimizing regenerative cooling channels for nuclear rocket engines is extremely limited. Salamon et al. [11] compared four regenerative cooling channel path shapes in nuclear thermal engines: straight, bifurcated, spiral, and sinusoidal. The results indicated that, under identical coolant mass flow rates, the sinusoidal and bifurcated

* Corresponding author. College of Astronautics, Nanjing University of Aeronautics and Astronautics, Nanjing, 211106, China.
** Corresponding author. Department of Nuclear Science and Technology, Nanjing University of Aeronautics and Astronautics, Nanjing, 211106, China.
*E-mail addresses:* zhaohangbin@nuaa.edu.cn (H. Zhao), tangxiaobin@nuaa.edu.cn (X. Tang).

https://doi.org/10.1016/j.ijthermalsci.2024.109201
Received 29 January 2024; Received in revised form 15 May 2024; Accepted 4 June 2024

**Nomenclature**

| | |
|---|---|
| $\boldsymbol{E}$ | total energy per unit mass of the coolant [kJ·kg$^{-1}$] |
| $\boldsymbol{f}$ | Mass force [m·s$^{-2}$] |
| k | Thermal conductivity [W·m$^{-1}$·K$^{-1}$] |
| *Nu* | Nusselt number |
| $\boldsymbol{P}$ | stress tensor [kg·m$^{-1}$·s$^{-2}$] |
| *PEC* | performance evaluation criteria |
| *Pr* | Prandtl number |
| *Re* | Reynolds number |
| S | internal heat source [W·m$^{-3}$] |
| ΔT | temperature difference [T] |
| $u$ | Velocity of coolant [m·s$^{-1}$] |
| $\rho$ | Density of coolant [kg·m$^{-3}$] |

channels achieved the most effective cooling. However, the properties of the coolant used in the simulation were stationary, which may lead to a lack of authenticity. Mullin et al. [12] explored the benefits of sinusoidal cooling channels of nuclear rocket engines through experiment and CFD modeling. The findings indicate that an increase in the amplitude of the sinusoidal path correlates with improved heat transfer capabilities. In contrast, research on chemical rocket engines and scramjet engines is relatively abundant. Structural optimization by adopting ribs with different arrangements is a frequently used way to strengthen the cooling effect further. To enhance the heat transfer ability in the cooling channel of the scramjet combustor, Li et al. [13] investigated the effect of rib parameters on the heat transfer process. The results showed that the average temperature of the heated surface could be reduced by 390–511 K under the heat flux of 2.0 MW/m$^2$. However, a potential limitation of this approach was that the wall temperature near the rib remarkably increased. Chen [14] studied the effects of spherical protruding structure on the flow and heat transfer characteristics in the turbulent channel. The results showed that the average Nusselt number in the spherical region increased by six times. In line with Elmouazen's work on V-shaped rib [15], the simulation results showed that the maximum thermohydraulic performance could be enhanced by 23 %. Following the research of Shanmugam [16], the arc-shaped ribs could effectively enhance the heat transfer performance. The maximum enhancement was considerably higher than the V-shaped rib and cylindrical ribs. Moreover, the aspect ratio of the cross-section of the rectangular cooling channel had an important influence on the flow and heat transfer characteristics in the cooling channel. Pizzarelli et al. [17] analyzed the heat transfer process in a rectangular channel with a large aspect ratio. The results showed an optimal aspect ratio of the cooling channel, which could not only meet the cooling requirements but also reduce the flow resistance. In addition, Song et al. [18] applied the pyramid lattice structures to the regenerative cooling channel. The numerical results showed that the pyramid lattice structures could form a high turbulent kinetic energy region, thus the convective heat transfer was enhanced. However, the pressure drop was sharply raised in comparison with that of the traditional smooth channel. Therefore, adopting a rib to strengthen the thermal protection ability of the nuclear rocket engine is crucial.

Current research is insufficient to accurately simulate and optimize the heat transfer processes within the cooling channels of nuclear thermal engines. Additionally, the diverse designs employed in chemical rocket engines and scramjet engines could provide valuable insights. The aim of this research is to investigate the effect of rib structure on the thermal protection ability of the nuclear rocket engine nozzle. The influences of the straight rib on the heated wall temperature and the pressure drop of the channel are analyzed. Additionally, the streamlined rib and the side rib are proposed and examined. On the basis of the results, two new composite rib structures are designed and analyzed in the straight channel. The influences of two types of composite ribs are further investigated in the bending channel.

## 2. Numerical model

### 2.1. Geometry

A typical nuclear rocket engine nozzle structure is shown in Fig. 1. In this structure, regenerative cooling channels are arranged around the nozzle. The heat from the nozzle wall is removed by the supercritical hydrogen that flows within the channels. In this design, the size of the rectangular cross section is much smaller than the size of the length. Moreover, the main zone is located near the throat, where the curvature of the channel is relatively large. Hence, the channel can be considered as straight with rectangular cross-section. Specifically, the straight rectangular cross-section channel is designated as the computational domain [19]. Given that the structure of the cooling channel is symmetrical, half of the structure is adopted for calculation. Hence, the computational cost can be reduced. As shown in Fig. 2, five types of ribs that arranged in the straight channel are studied separately: straight rib (Fig. 2a), streamlined rib (Fig. 2b), side rib (Fig. 2c), straight composite rib (Fig. 2d) and streamlined composite rib (Fig. 2e). The arrows in Fig. 2a and f represent the coolant flow direction of the straight channel and bending channel, respectively. The test straight channel is 2 mm*16 mm*100 mm and the bending channel is 2 mm* 16 mm* 1516 mm. The thickness of the side wall represents the half of the distance between two adjacent channels.

The straight and streamlined ribs are located at the bottom of the channel. Thus, the bottom rib refers to the straight rib and streamlined rib. The side rib is located at the sidewall. Particularly, the straight composite rib is formed by one straight rib and two side rib. The streamlined composite rib, similar to the straight composite rib, consisted of one streamlined rib and one side rib. In addition, as shown in Fig. 2f, the influences of two kinds of composite ribs in the bending channel are comparatively studied.

### 2.2. Numerical method

The boundary condition at the inlet is characterized by the mass flow inlet. The mass flow rate is maintained at 0.015 kg/s, unless otherwise stated.

The outlet is set as pressure outlet. Both sides of the model are symmetrical boundaries. A constant heat flux of 57 MW/m$^2$ is applied to the bottom wall, and the rest of walls are all adiabatic. More detailed parameters of straight channel and bending channel are shown in Table 1 and Table 2, respectively [10].

The thermal properties of supercritical hydrogen under the pressure of 19 MPa are shown in Table 3. A zirconium copper alloy which is widely used in rocket engine nozzle is adopted as the material of the wall. Its main properties are listed in Table 4. The fitted polynomial curves of properties are shown in Fig. 3.

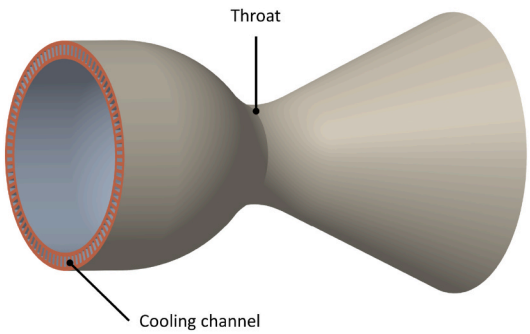


**Fig. 1.** Schematic of the nozzle.

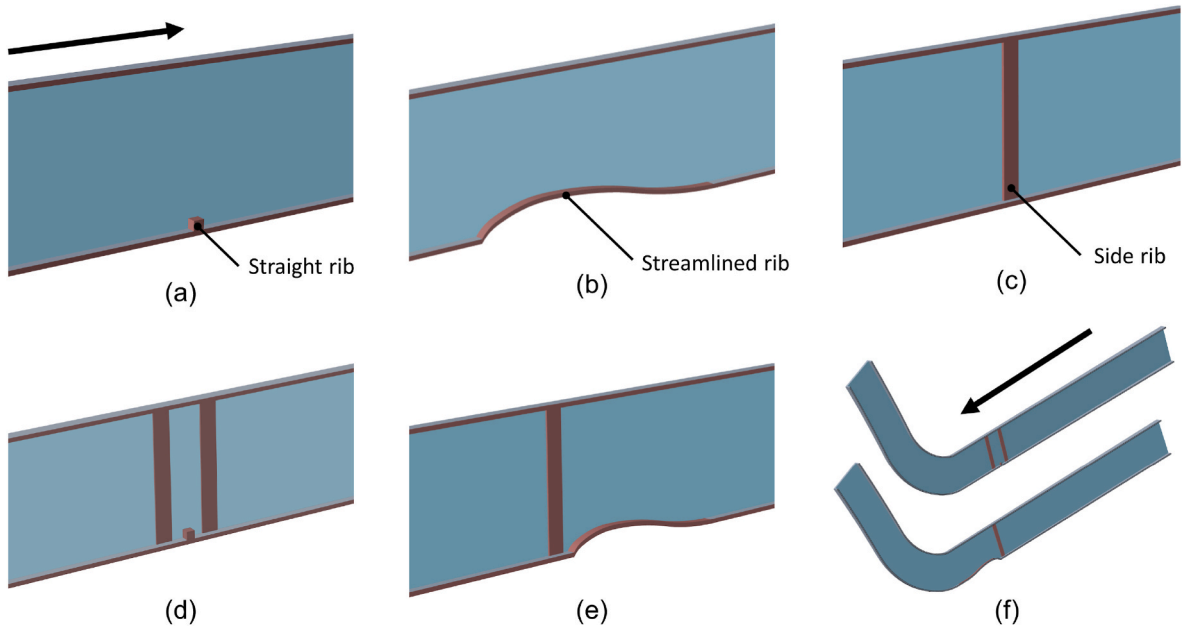


**Fig. 2.** Channel with rib: (a) straight rib; (b) streamlined rib; (c) side rib; (d) straight composite rib; (e) streamlined composite rib; (f) composite rib in the bending channel.

**Table 1**
Parameters of the straight channel.

| Parameter | value |
|---|---|
| Inlet pressure/MPa | 19.41 |
| Inlet temperature/K | 37 |
| Width/mm | 2 |
| Inner wall thickness/mm | 0.5 |
| Outer wall thickness/mm | 0.5 |
| Side wall thickness/mm | 1 |

**Table 2**
Parameters of bending channel.

| Parameter | value |
|---|---|
| Inlet pressure/MPa | 19.41 |
| Inlet temperature/K | 37 |
| General width/mm | 2 |
| General height/mm | 16 |
| Outer wall thickness/mm | 0.5 |
| Inner wall thickness/mm | 0.5 |
| General side wall thickness/mm | 1 |

The structure of the bending channel used for the nuclear rocket nozzle can be found in Ref. [8]. Details of the meshing are shown in Fig. 4. The hexahedral cell-based unstructured mesh is constructed by ICEM-CFD. The minimum meshing quality is more than 0.9. In the vicinity of the ribs, the y + values range from 1 to 5, thereby satisfying the requirements of the SST $k$-$\omega$ model effectively. The numerical process is operated via Ansys Fluent. The SIMPLE method is adopted to solve the pressure-velocity coupling.

The flow of supercritical hydrogen in the regenerative cooling channel satisfies the Naiver-Stokes equations:

$$\frac{\partial(\rho u_i)}{\partial x_i} = 0 \tag{1}$$

$$\frac{\partial(\rho u_i u_j)}{\partial x_i} = \rho \boldsymbol{f}_j + \frac{\partial \boldsymbol{P}}{\partial x_j} \tag{2}$$

**Table 3**
Thermal properties of supercritical hydrogen.

| Parameter | value | range |
|---|---|---|
| Density/kg·m$^{-3}$ | −6.11462e-6T$^3$+0.00429464T$^2$-1.0544T + 107.65 | 30K–300K |
| | −2.8746e-8T$^3$+7.455031e-5T$^2$-0.0700213T + 28.5549 | 300K–1000K |
| Specific Heat/ J·kg$^{-1}$·K$^{-1}$ | 0.01940539T$^3$-5.57905T$^2$+523.267T-1974.67 | 30K–120K |
| | 9.87361e-7T$^4$-9.64917e-4T$^3$+0.32078T$^2$-38.08674T + 15307.71939 | 120K–350K |
| | −1.5728e-7T$^3$+0.0023391T$^2$-2.49069T + 15316.26 | 350K–1000K |
| Thermal Conductivity/ W·m$^{-1}$·K$^{-1}$ | −1.33968e-8T$^3$+8.931196e-6T$^2$-0.001371097T + 0.180105 | 30K–200K |
| | 0.0003830752T + 0.0870992 | 200K–1000K |
| Viscosity/kg·m$^{-1}$·s$^{-1}$ | 1.106886e-13T$^4$-6.06889e-11T$^3$+1.21794e-8T$^2$-1.052e-6T+3.93263e-5 | 30K–200K |
| | 1.661041e-8T+4.388086e-6 | 200K–1000K |

**Table 4**
Thermal properties of zirconium copper alloy.

| Parameter | value | range |
|---|---|---|
| Density/kg·m$^{-3}$ | 8890 | 30K–1200K |
| Specific Heat/J·kg$^{-1}$·K$^{-1}$ | 393.5 | 30K–1200K |
| Thermal Conductivity/ W·m$^{-1}$·K$^{-1}$ | 2.8602e-11T$^6$-3.5577e-8T$^5$+1.787201e-5T$^4$-0.0046481T$^3$ +0.6666122T$^2$-51.4513T + 2160.963 | 30K–300K |
| | −0.06T + 403 | 300K–1200K |

$$\frac{\partial(\rho u_i E)}{\partial x_i} = \rho \boldsymbol{f}_i \cdot u_i + \frac{\partial(\boldsymbol{P} \cdot u_i)}{\partial x_i} + \frac{\partial(k\Delta T)}{\partial x_i} + S \tag{3}$$

where $\boldsymbol{u}$ represents the velocity of the fluid, $\boldsymbol{f}$ is the volume force in the fluid, and $\boldsymbol{P}$ is the surface force.

For the forced convective heat transfer in the channel, the criterion is adopted to quantifies the effectiveness of heat transfer:

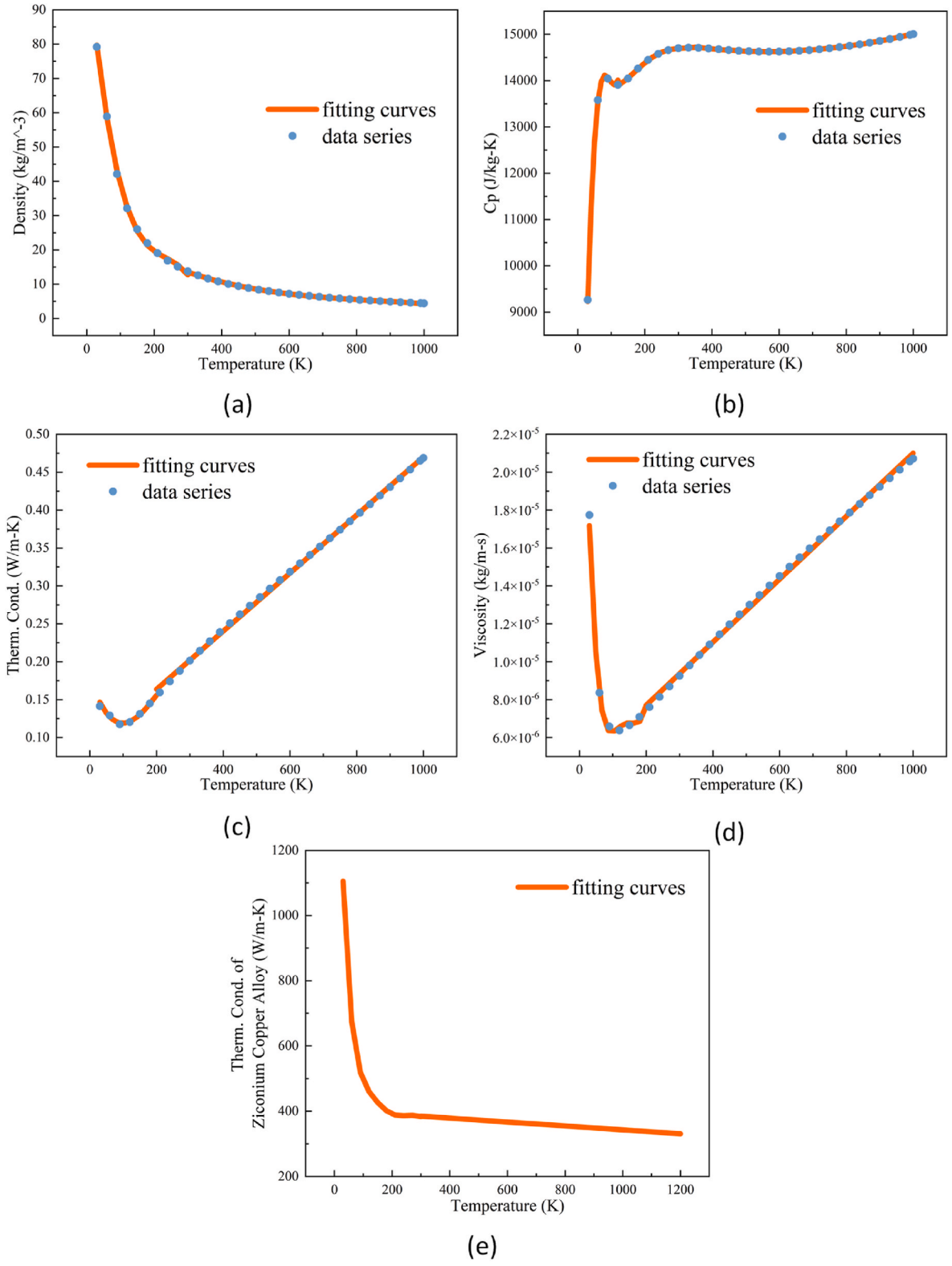


**Fig. 3.** Thermal properties of supercritical hydrogen and zirconium copper alloy.

$$Nu = 0.021 Re^{0.8}\, Pr^{0.4} \left(\frac{Pr_w}{Pr}\right)^{0.25} \tag{4}$$

where *Re*, *Pr*, and *Nu* take the body temperature of the fluid as the qualitative temperature, and $Pr_w$ is the Prandtl number with the wall temperature as the qualitative temperature.

The performance evaluation criteria (*PEC*) are adopted to evaluate the comprehensive effects of flow and heat transfer performance:

$$PEC = (Nu_c / Nu_s) \Big/ (f_c/f_s)^{1/3} \tag{5}$$

where $Nu_c$ and $f_c$ represents the Nusselt number and friction factor of the

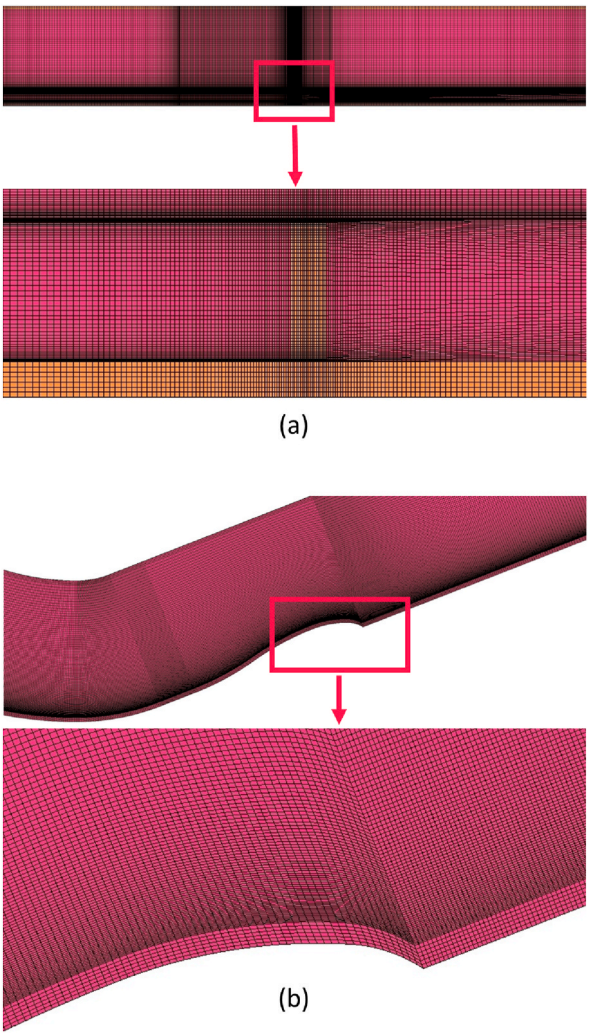


**Fig. 4.** Gird of (a) the straight channel and (b) the bending channel.

channel with rib, and $Nu_s$ and $f_s$ represents the Nusselt number and friction factor of the traditional smooth channel.

In this research, the coolant mainstream exhibits a high Reynolds number. SST $k$-$\omega$ model has good simulation accuracy for the boundary layer and large Reynolds number flow on the wall [20], thus, the SST $k$-$\omega$ model is adopted as the turbulence model. The turbulent kinetic energy $k$ and specific dissipation rate $\omega$ in the SST $k$-$\omega$ model can be calculated as follows:

$$\frac{\partial(\rho k)}{\partial t}+\frac{\partial(\rho u_j k)}{\partial x_j}=\tau_{ij}\frac{\partial u_i}{\partial x_j}-\beta^*\rho\omega k+\frac{\partial\left[(\mu+\sigma_k\mu_t)\frac{\partial k}{\partial x_j}\right]}{\partial x_j} \tag{6}$$

$$\frac{\partial(\rho\omega)}{\partial t}+\frac{\partial(\rho u_j\omega)}{\partial x_j}=\frac{\gamma}{\nu_t}\tau_{ij}\frac{\partial u_i}{\partial x_j}-\beta\rho\omega^2+\frac{\partial\left[(\mu+\sigma_\omega\mu_t)\frac{\partial k}{\partial x_j}\right]}{\partial x_j}+2(1-F_1)\frac{\rho\sigma_{\omega 2}}{\omega}\frac{\partial k}{\partial x_j}\frac{\partial\omega}{\partial x_j} \tag{7}$$

Where $\tau_{ij}$ is the Reynolds stress tensor, $\mu$ is the molecular viscosity and $\mu_t$ is the turbulent viscosity.

### 2.3. Model validation

The case that straight channel with 1 mm straight rib was selected for checking the gird sensitivity. Seven sets of Computational meshes were tested. The number of meshes are 63,000, 140,000, 320,000, 660,000, 1,300,000, 2,590,000, 5,380,000 respectively.

Similar to Fig. 4a, the local encryption of meshes is performed in the vicinity of the ribs. As shown in Fig. 5, results apparently reveal that the deviation between heated wall average temperature of model with 1,300,000 grids and 5,380,000 grids below 0.1 %. When the number of grids is greater than 1300,000, the temperature no longer changes significantly.

Since the experimental results of supercritical hydrogen flow in the regenerative cooling channel could not be found in the open literature, the circular tube adopting supercritical hydrogen as coolant is to verify the reliability. In this test case, inlet temperature is 25 K, and the back pressure is set as 4.95 MPa. The heated straight tube has a length of 914.4 mm and an internal diameter of 8.509 mm, with only the last two-thirds of the tube being electrically heated. The SST $k$-$\omega$ model is consistently employed as the turbulence model throughout the study. Further details regarding the test model and its boundary conditions can be found in Ref. [21].

Fig. 6 illustrates the comparison between the computed and experimental temperature of the heated wall. It can be concluded that the numerical results agree well with the experimental results, although the experimental data slightly higher than the numerical results at the peak.

## 3. Flow and heat transfer characteristics of the straight channel

As shown in Table 1, the parameters of the regenerative cooling channel are chosen in accordance with the 100-ton nuclear rocket engine system [10].

The combination structure of the bottom and side ribs are shown in Fig. 2. As shown in this figure, the straight and streamlined types of the bottom rib are placed in the heated wall, and the side ribs are placed in the sidewalls. The height of these ribs has substantial influence on the flow and heat transfer of the coolant. To investigate the differences of the impact among the height of these ribs, each rib is simulated separately. The streamlined ribs of other heights are enlarged/reduced proportionally.

### 3.1. Straight channel with bottom rib

The average temperature and maximum temperature of the heated wall of two kinds of bottom ribs are shown in Fig. 7a. For the streamlined rib, the abscissa means the height of the streamlined rib at x = 50 mm, which is the center of the straight channel.

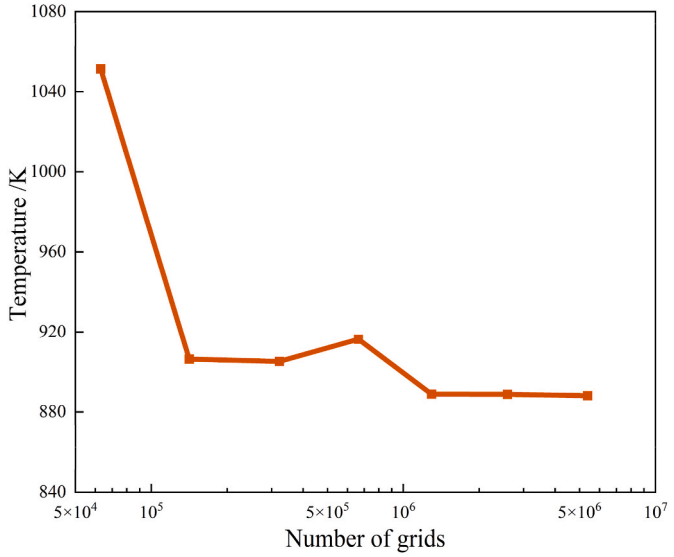


**Fig. 5.** Grid-independence validation.

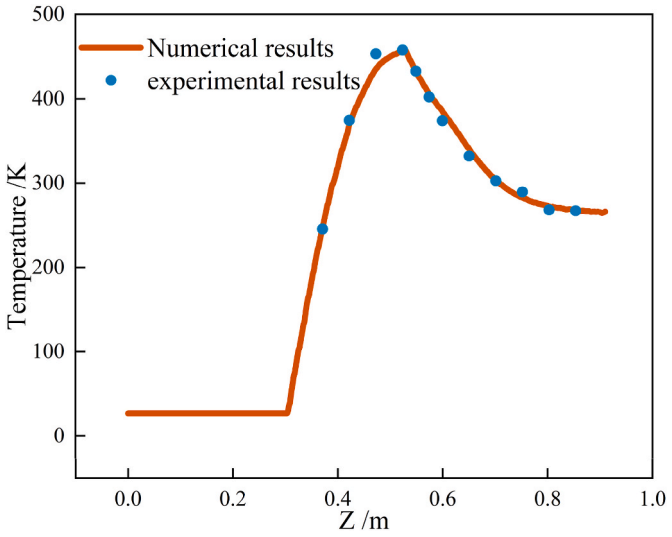


**Fig. 6.** Comparison between the computed and experimental temperature of the heated wall.

Fig. 7a shows that the maximum temperature generally increases as the rib height increases from 0 mm to 3 mm. For the straight rib, the maximum temperature and the average temperature are higher than that of the streamlined rib. When the rib height exceeds 1.5 mm, the maximum temperature remarkably rises.

The pressure drop of the straight and streamlined rib are shown in Fig. 7b. As the height increases from 0 mm to 3 mm, the pressure drop of both ribs increases exponentially. The pressure drop of the streamlined rib escalates more significantly than that of the straight rib with the increase in height. As for the streamlined rib, the maximum temperature slightly grows with the increase in height. Additionally, in contrast to the straight rib, the average temperature marginally declines as the height rises. As can be seen in Fig. 8, the maximum temperatures of two types of ribs occur in the nearby area of the rib. This phenomenon can be attributed to the distribution of the coolant.

When the rib is excessively high, a substantial quantity of coolant is distanced from the heated wall due to the rib's effect. This results in a reduced amount of coolant and a lower velocity swirl flow in the vicinity of the rib, as illustrated in Fig. 9. The flow distribution leads to the increase in the maximum temperature of the wall. Fig. 10 shows that the enhancement on turbulence caused by the streamlined rib is weaker than that caused by the straight rib, but the decrease in wall average temperature is larger than that of the straight rib.

### 3.2. Straight channel with side rib

The effect of the side rib arranged on the side wall of the channel is investigated. As shown in Fig. 2, the height of the side rib is the same as the height of the channel, and the width is 2 mm. Fig. 11 illustrates the variation of wall temperature and channel pressure drop with rib height. In contrast to the bottom rib, the maximum wall temperature and average temperature decrease with the increase in the height of the side rib.

As shown in Fig. 12, when the height of the side rib is greater than 0.2 mm, the temperature near the side rib can be effectively reduced. Nevertheless, in comparison to the bottom rib, the pressure drop sharply escalates with the rise in the rib's height. This is attributed to the fact that an increase in the height of the side rib can intensify the turbulent kinetic energy more dramatically (Fig. 13). Moreover, the influence area of the side rib includes the upper part of the channel. The computational result of Nusselt number in all considered types are plotted in Fig. 14, in which the straight horizontal line is the Nusselt number of the channel without ribs.

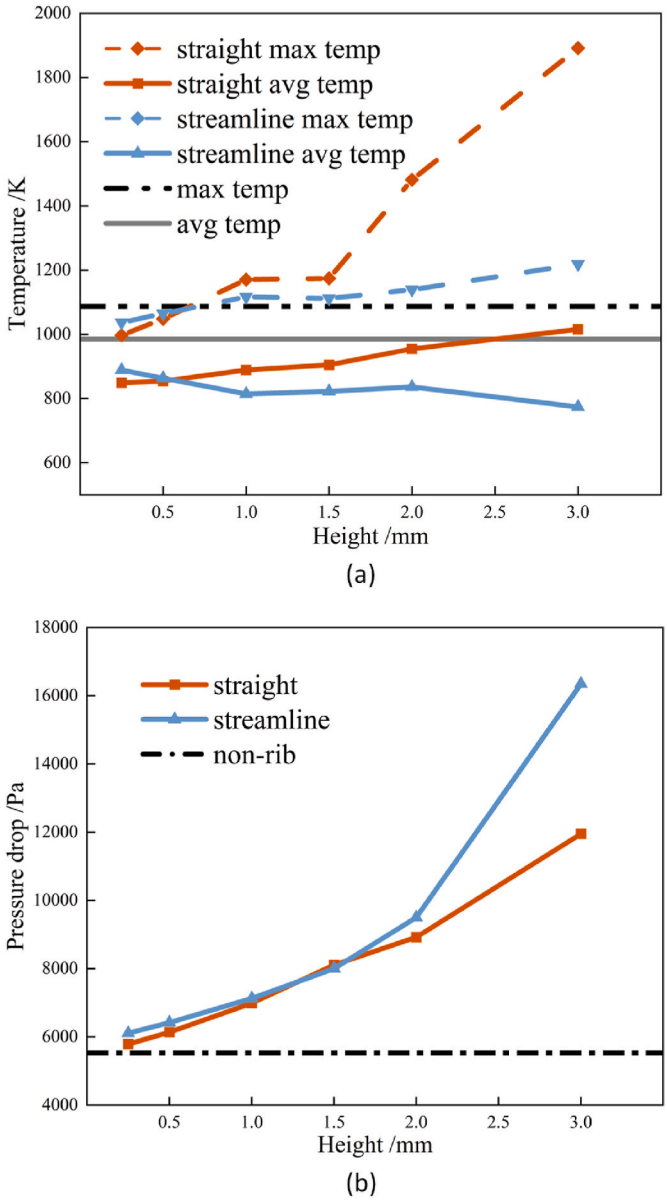


**Fig. 7.** (a) Temperature at heated wall of the straight channel with straight rib and (b) pressure drop of the straight channel with a straight rib.

The increase in the height of the bottom rib remarkably increases the *Nu*, whereas the height of the side rib has a minimal impact on it. This outcome could be attributed to the positional differences between these two types of ribs. The straight and streamlined ribs are much closer to the heat flux surface than that of the side rib. As a result, the Reynolds number of the straight rib and streamlined rib is considerably large.

Fig. 15 exhibits the effects of height on *PEC* for different types of rib. The *PEC* of the bottom ribs declines with increasing height. This is because the resistance loss becomes much stronger than the enhancement of heat transfer, especially when the height exceeds 2 mm. The bottom rib achieves a comparatively high *PEC* when the height is less than 1 mm. The *PEC* of the side rib also decreases with increasing height, for the same reason as the bottom rib. Additionally, the *PEC* of the side rib is greater than 0.8 only when the height is less than 0.1 mm.

### 3.3. Straight channel with composite rib

In accordance with the above analysis, the effect of the rib height on wall temperature distribution and turbulent mixing were

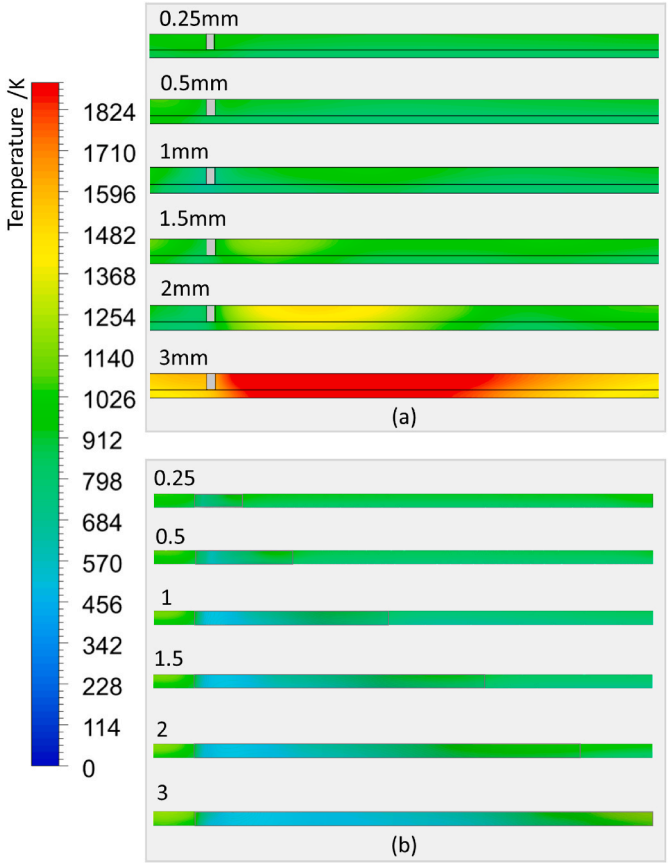


**Fig. 8.** Comparison of the heated wall temperature distribution between (a) the straight rib and (b) the streamlined rib.

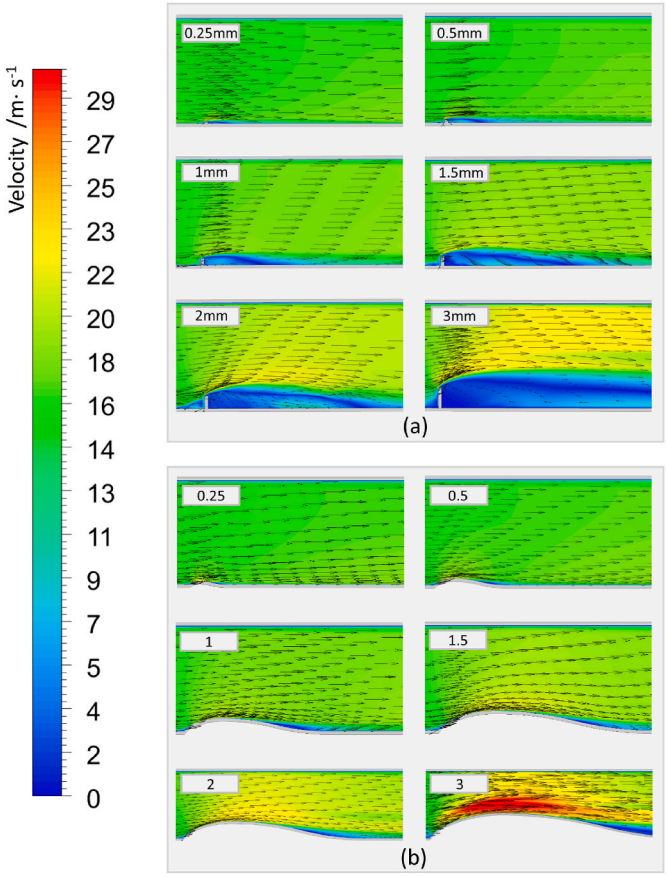


**Fig. 9.** Comparison of the velocity distribution between (a) the straight rib and (b) the streamlined rib.

comprehensively considered. Thus, to further enhance the convective heat transfer by modifying the secondary flow and escalating turbulence intensity, a composite rib structure has been designed, as shown in Fig. 2d and e. In the design of straight composite rib, the height of the straight rib is 1 mm and the height of the side rib is 0.2 mm. For the streamlined composite rib, the height of the streamlined rib is 1 mm, and the height of the side rib is 0.2 mm.

On the basis of the design, the influence of the distance between the side rib and the bottom rib on the flow and heat transfer in the cooling channel is analyzed. In Fig. 16, the distance in abscissa refers to the distance between the center of the side rib and the straight rib in the flow direction. For the streamlined rib, the position for calculating the distance is where the height relative to the bottom is 1 mm.

The variation of maximum temperature and average temperature of the composite rib with the rib distance is shown in Fig. 16. For the straight composite rib, when the side rib and the straight rib are combined (at a distance of 1 mm), the maximum temperature and average temperature on the heated wall clearly increase. Fig. 17 shows the temperature distribution of the heated wall. The temperature of the heated wall located directly beneath the rib is significantly higher than the temperature in other areas.

As shown in the velocity vector diagram, the mass flow rate of the coolant near the heated wall is slight (Fig. 18), although the turbulent kinetic energy increases greatly in the area near the ribs (Fig. 19). On the one hand, as shown in Fig. 18, when the distance between the side rib and the bottom rib is greater than 3 mm, the low velocity region near the rib is greatly reduced. Fig. 19 illustrates that when the distance is larger than 3 mm, the region with larger turbulent kinetic energy is closer to the heat flux wall. As the distance is further increased, the coupling effect of the two kinds of ribs steep falls.

As shown in Fig. 17, when the rib distance is 5 mm, the temperature near the rib increases, and the area of the low temperature region decreases remarkably compared with the condition when the rib distance is 3 mm. On the other hand, for the streamlined composite rib, the effect of rib distance on heat transfer optimization is smaller than that of the straight composite rib. However, for the straight composite rib, the temperature in the front area of the bottom ribs (the maximum temperature) decreases with the separation of the ribs. Based on the above analysis, the composite rib not only remarkably increases the turbulence of the flow field, which can enhance the heat transfer on a large scale, but also considerably reduces the temperature near the rib. The straight composite rib has an optimal distance between the ribs, which range from 3 mm to 4 mm. For the streamlined composite rib, the heat transfer optimization effect is not sensitive to the distance, and the pressure drop loss is smaller than that of the straight composite ribs (Fig. 16).

Fig. 20 exhibits the effects of distance on *Nu* and *PEC*. Fig. 20 (a) indicates that the heat transfer enhancement of the straight composite rib is greater than that of the streamlined composite rib. However, the *PEC* of the straight composite rib is generally lower than that of the streamlined composite rib. This is primarily because the resistance loss of the streamlined composite rib is much smaller than that of the straight composite rib. Comparing the single rib, it is found that the *Nu* for the straight composite rib exceeds that of the 3 mm straight rib (Fig. 14) when the distance between them is approximately 2–3 mm. Additionally, the *PEC* of the straight composite rib is significantly higher under these conditions. Furthermore, both the *Nu* and the *PEC* reach their peak values when the distance between the straight rib and the side rib is 2 mm.

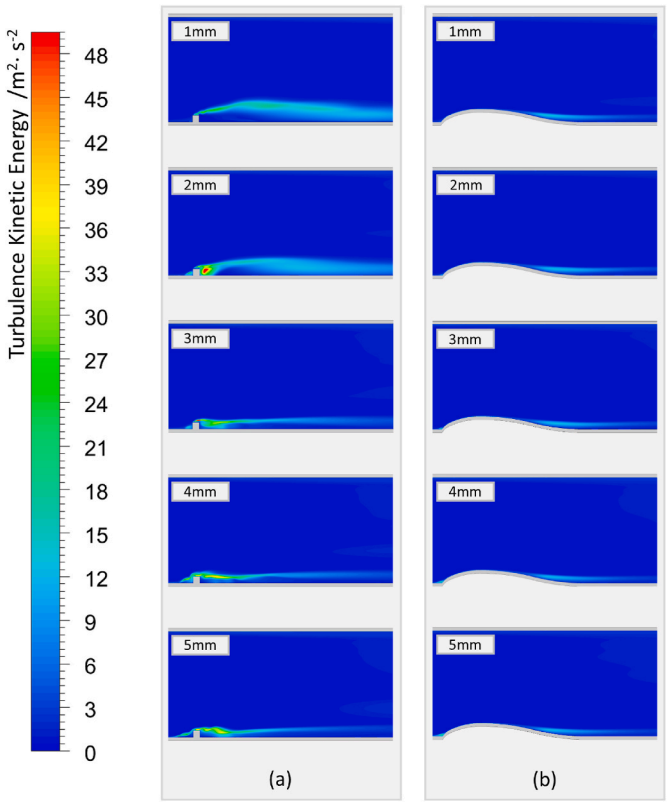


**Fig. 10.** Comparison of the turbulence kinetic energy distribution between (a) the straight rib and (b) the streamlined rib.

## 4. Flow and heat transfer characteristics of the bending channel

To further verify the heat transfer optimization effect of the composite rib structure on the throat region, the regenerative cooling channel in the throat area is modeled according to the design parameters of the nuclear rocket engine nozzle in Ref. [9].

This model considers the influence of the channels on either side, with symmetric surfaces present on both sides of the channel. The bottom wall of the channel is designated as the heated wall. The heat flux distribution is modeled based on the data calculated in Ref. [9], and the heat flux changes along the axial direction of the nozzle. Other parameters of the bend channel are shown in Table 2.

### *4.1. Bending channel with the straight composite rib*

In accordance with the characteristics of the straight ribs in the above analysis, the straight composite rib is arranged in front of the throat area. Fig. 21 shows that the highest temperature of the heated wall appears at the end of the section. For the traditional smooth structure, the highest temperature is 1132 K, and the average temperature is 631.9 K. When the composite rib is arranged, the maximum temperature at the end of the section decreases to 1037 K, and the average temperature of the heat flux wall decreases to 598 K. Fig. 22 illustrates the heated wall temperature of the channel with the straight composite rib. The wall temperature near the rib marginally decreases, which may prove that in the bending channel, the arrangement of the side rib can considerably enhance the heat transfer in the nearby area.

The turbulent kinetic energy of the bending channel with a straight composite rib is shown in Fig. 23. Similar to the straight channel, the contour is in the center plane of the geometry. The turbulent enhancement is analogous to that of the straight channel. Both turbulent kinetic energy increase to 30 $m^2/s^2$. In addition, the pressure drop between the inlet and outlet of the channel of the channel increases from 8458 Pa to

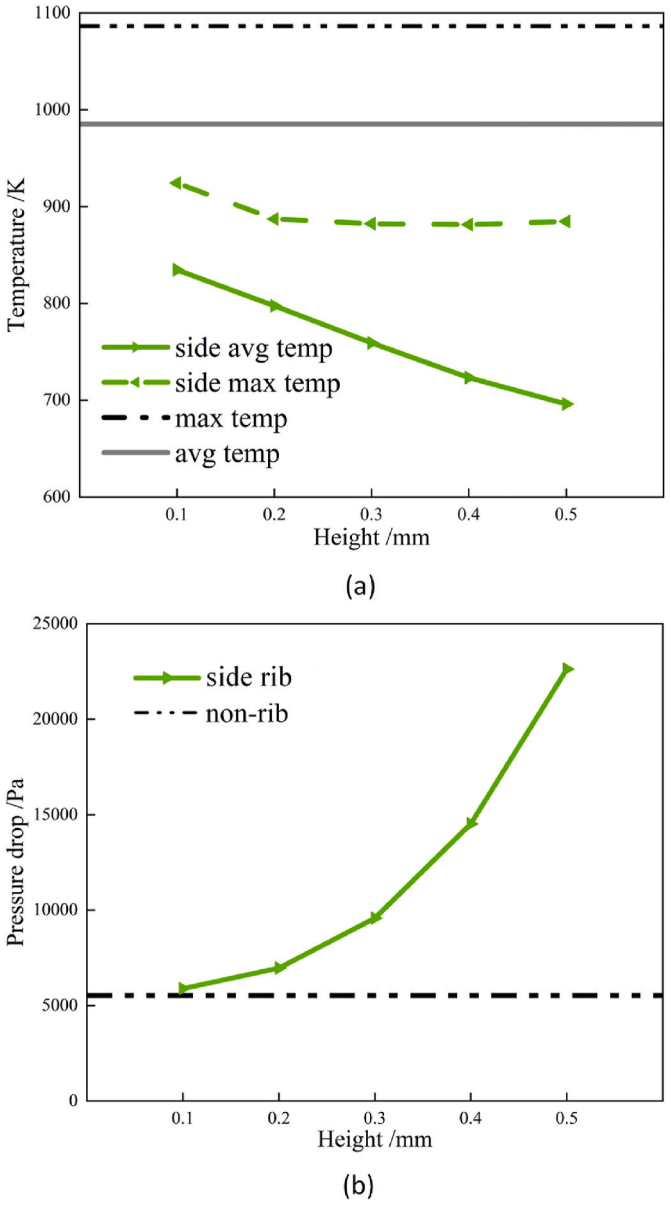


**Fig. 11.** (a) Temperature of the straight channel with a side rib and (b) pressure drop of the straight channel with a side rib.

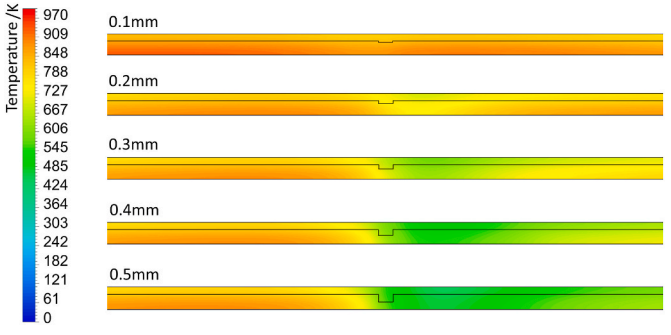


**Fig. 12.** Heated wall temperature distribution of the straight channel with a side rib.

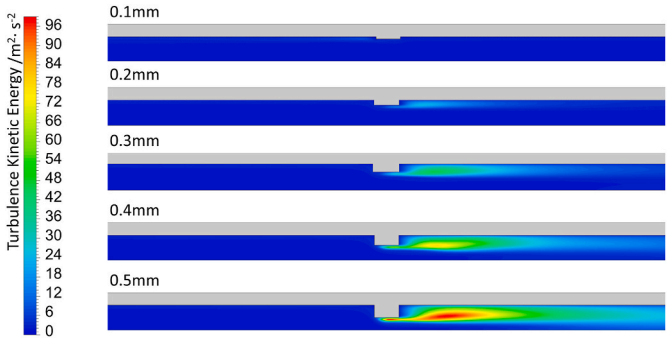


**Fig. 13.** Turbulence kinetic energy distribution of the straight channel with a side rib.

10390 Pa, which is lower than that of the straight channel.

### 4.2. *Bending channel with the streamlined composite rib*

The wall temperature of the bending channel with a streamlined composite rib and the bending channel with a composite streamlined rib is shown in Fig. 24. As shown in this figure, the streamlined composite rib (Fig. 24b) is set in the same position as the straight composite rib (Fig. 24a).

The maximum temperature of the streamlined composite rib is much higher than that of the straight composite rib. Moreover, its maximum temperature even exceeds the maximum temperature of the normal smooth channel.

Fig. 25 illustrates the heated wall temperature of the channel. The temperature in the front region of the streamlined rib can be considerably reduced. On the basis of this characteristic, the streamlined composite rib is arranged at the end of the channel, as shown in Fig. 26. However, the arrangement of the streamlined composite rib further increases the maximum temperature at the end of the channel to 1333 K.

The temperature at the front of the streamlined rib decreases due to the side rib, and the average temperature of the heat flux wall is reduced. In connection with the analysis in Fig. 24, the velocity at the front of the streamlined rib is remarkably higher than that in the traditional smooth channel (see Fig. 27). However, the velocity decreases in the back region of the streamlined rib, which makes the highest temperature appears in this region. Consequently, the decrease in flow velocity further increases

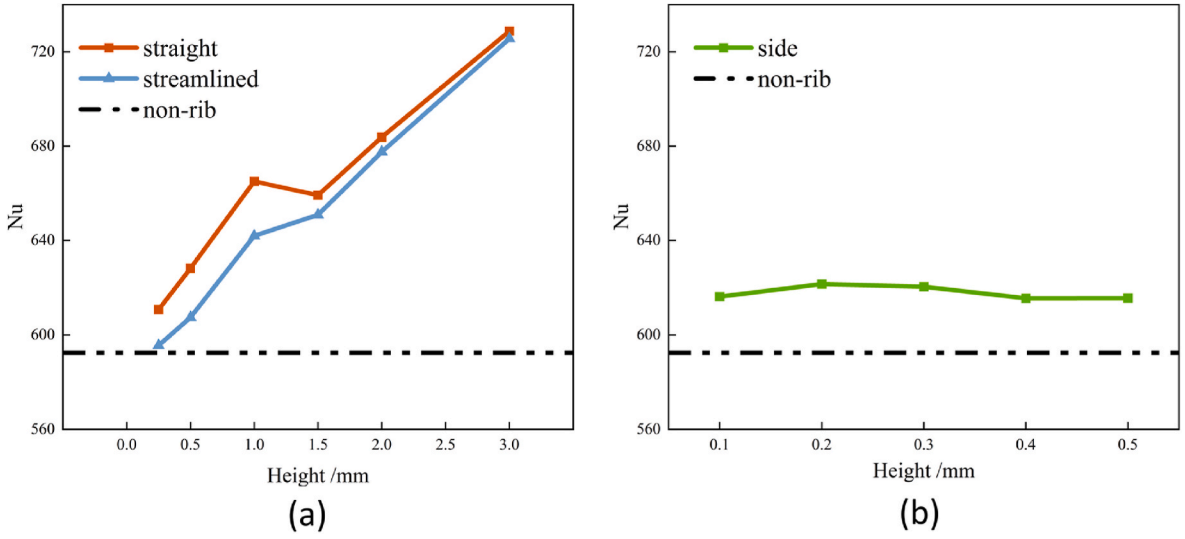


**Fig. 14.** The Nusselt number with the height of (a) straight, streamlined and (b) side ribs.

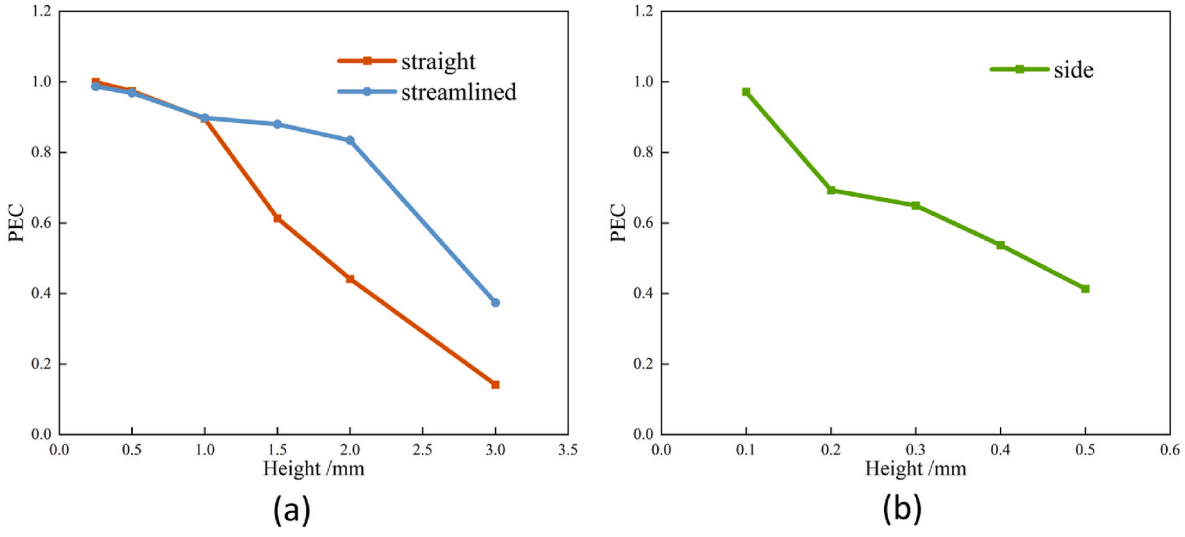


**Fig. 15.** The *PEC* with the height of (a) straight, streamlined and (b) side ribs.

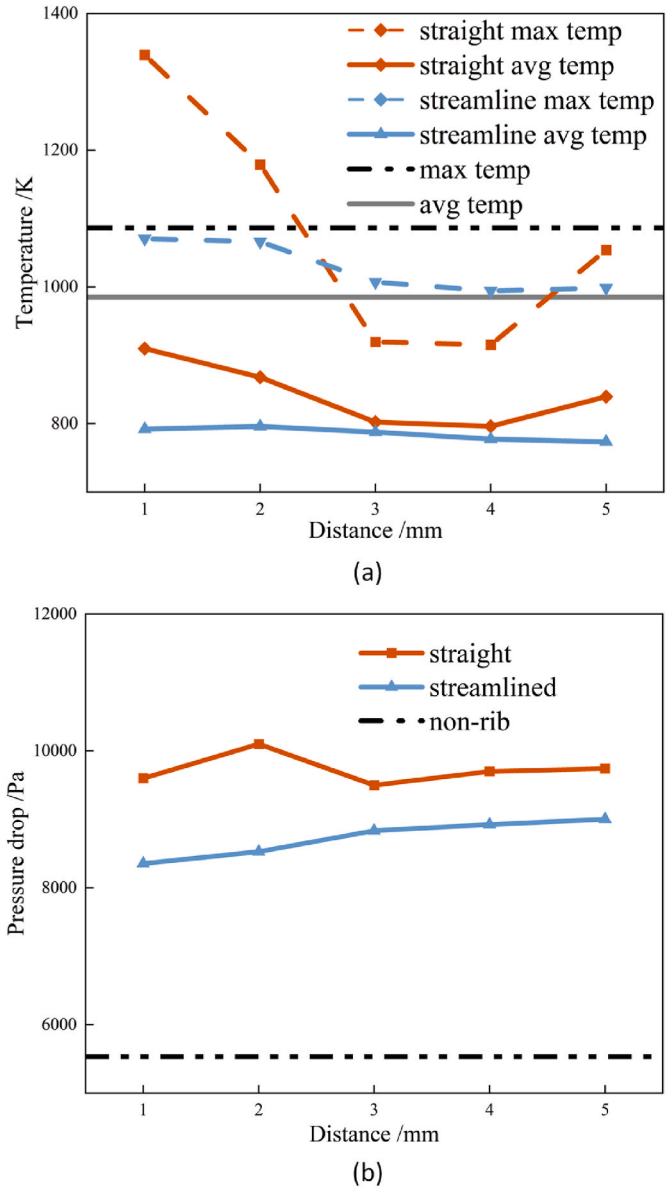


**Fig. 16.** (a) Temperature of the straight channel with composite ribs and (b) pressure drop of the straight channel with composite ribs.

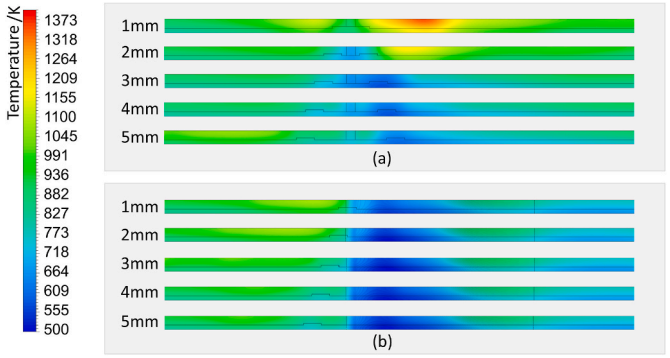


**Fig. 17.** Comparison of the heated wall temperature distribution between (a) the straight composite rib and (b) the streamlined composite rib.

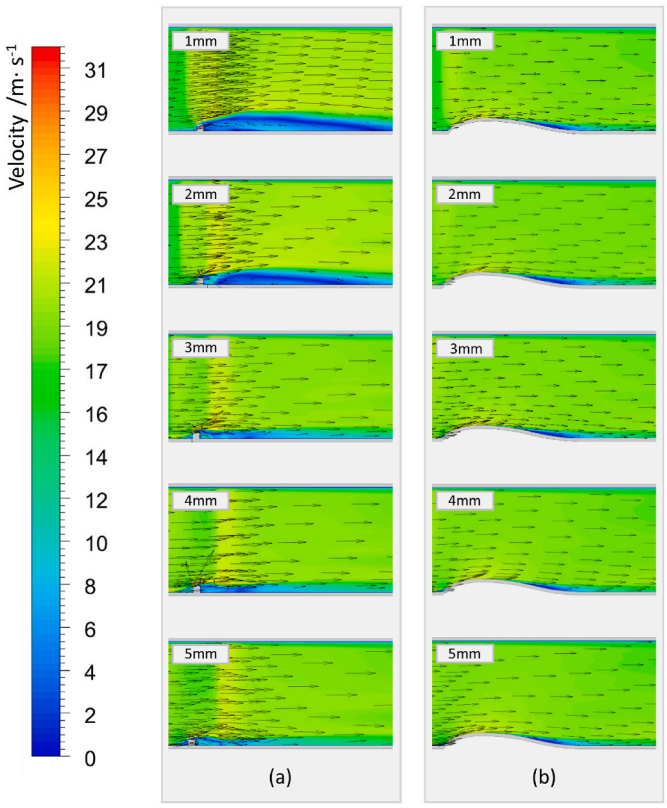


**Fig. 18.** Comparison of the fluid symmetry velocity distribution between (a) the straight composite rib and (b) the streamlined composite rib.

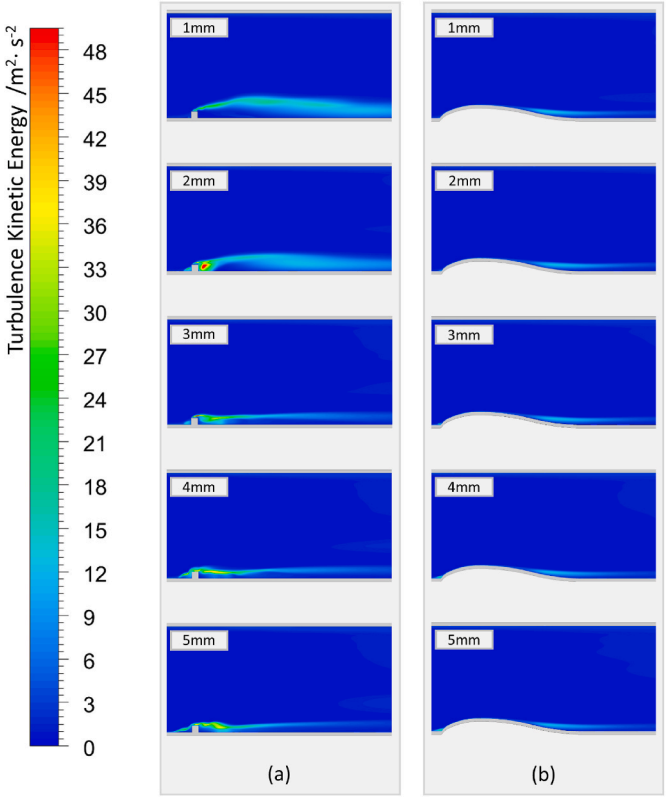


**Fig. 19.** Comparison of the fluid symmetry turbulence kinetic energy distribution between (a) the straight composite rib and (b) the streamlined composite rib.

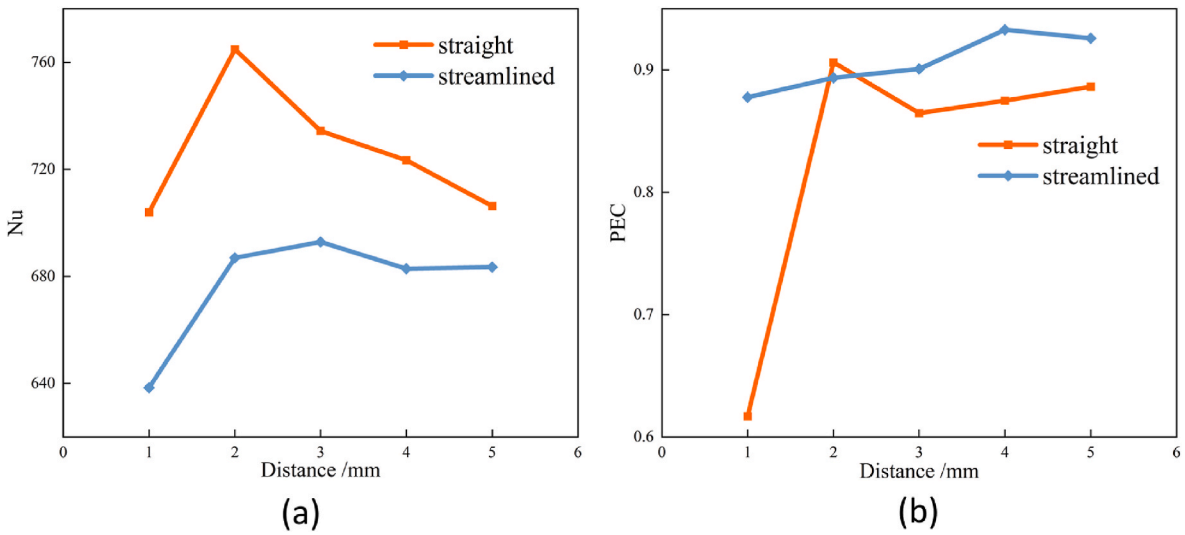


**Fig. 20.** (a) The Nusselt number and (b) the *PEC* with the composite ribs.

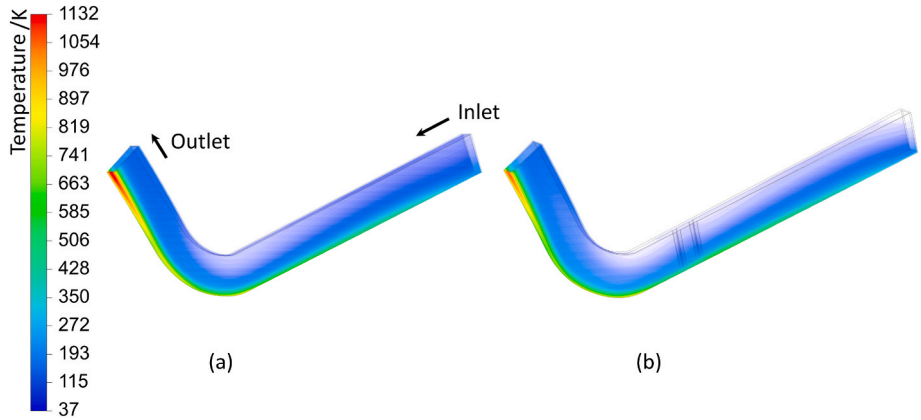


**Fig. 21.** Comparison of the wall temperature distribution between (a) the traditional smooth channel and (b) the channel with a straight composite rib.

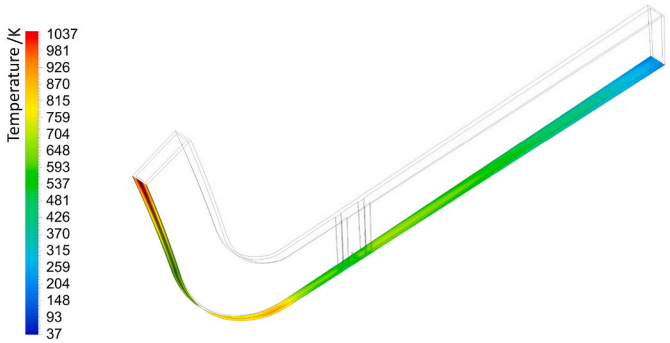


**Fig. 22.** Temperature distribution at the heated wall of the channel with a straight composite rib.

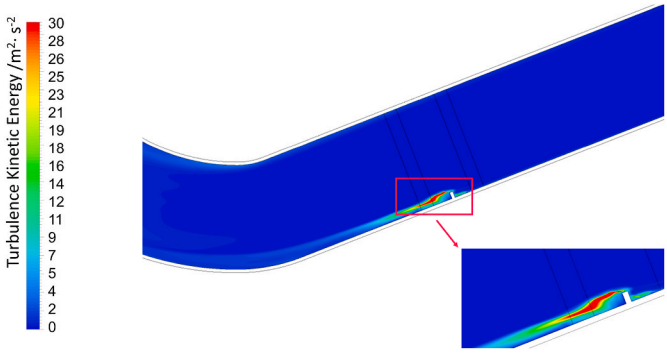


**Fig. 23.** Turbulent kinetic energy distribution at the center section of the bending channel with a straight composite rib.

the temperature in this area.

## 5. Conclusion

In this research, the effects of three different ribs on the flow and heat transfer characteristics in the regenerative cooling channel were studied. Two composite rib structures with the combination of side rib, straight rib and streamlined rib were proposed and analyzed. Furthermore, the influence caused by the arrangement of two kinds of composite ribs in the bending channel were studied. The conclusions are as follows.

(1) When the rib height exceeds 1.5 mm, the vortex velocity on both sides of the straight rib and upstream of the streamlined rib becomes relatively low, leading to a considerable increase in wall temperature. With the increase of the bottom rib height, the *Nu*

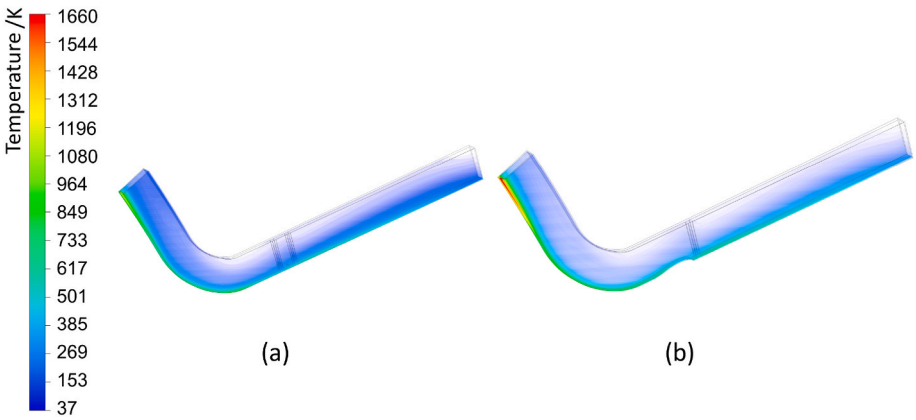


**Fig. 24.** Comparison of the wall temperature distribution between (a) the channel with straight composite rib and (b) the channel with a streamlined composite rib.

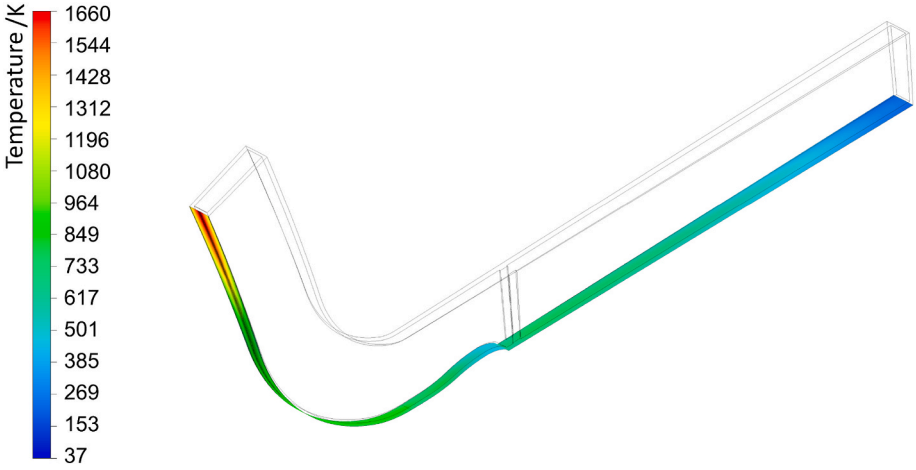


**Fig. 25.** Heated wall temperature distribution of the channel with a streamlined composite rib.

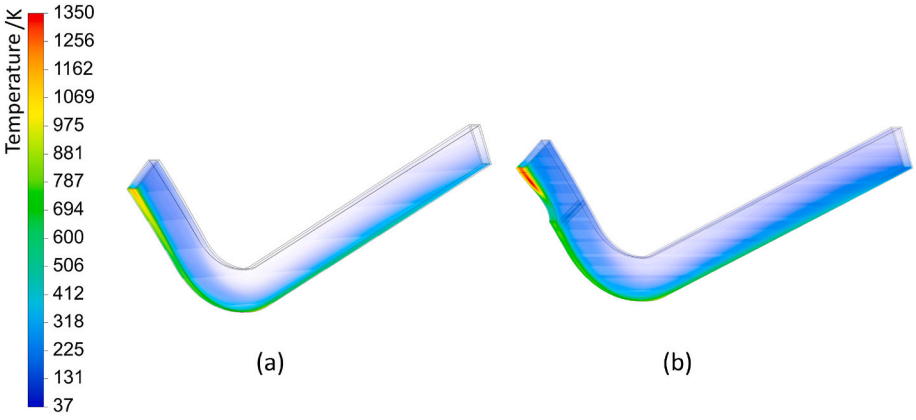


**Fig. 26.** Comparison of the wall temperature distribution between (a) the normal channel and (b) the channel with a streamlined composite rib.

significantly enhanced, while the *PEC* declines with greater rib height.

(2) The side rib can effectively lower the temperature of the heated wall in the area proximate to the rib. However, the turbulence intensity of the coolant exhibits a relatively modest increase. The increase of the rib's height markedly reduces the *PEC*, whereas the *Nu* remains consistent generally.

(3) When the distance between the side rib and the straight rib is approximately 3–4 mm, the straight composite rib structure can effectively reduce the temperature of the heated wall. In comparison to the single bottom rib structure, the composite rib structure can significantly enhance the *PEC* and *Nu*.

(4) The use of the straight composite rib in the bending channel can significantly reduce both the maximum temperature and average temperature. Moreover, the temperature proximate to the ribs exhibits a marginal decrease. However, the increase in turbulence intensity for the streamlined composite rib is minimal, resulting in effective temperature reduction in areas close to the rib.

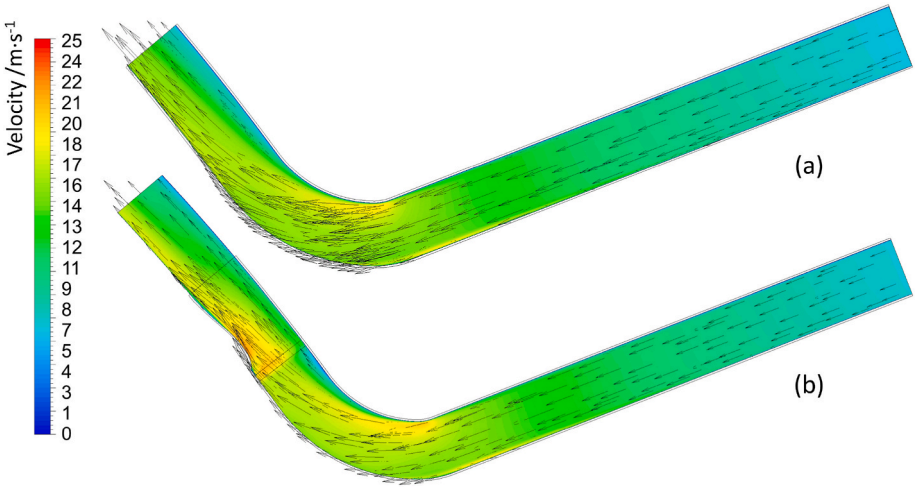


**Fig. 27.** Comparison of the velocity distribution between (a) the normal channel and (b) the channel with a streamlined composite rib.

## CRediT authorship contribution statement

**Si Yang:** Writing – original draft, Visualization, Validation, Software, Methodology, Investigation, Formal analysis, Data curation, Conceptualization. **Hangbin Zhao:** Writing – review & editing, Supervision, Resources, Project administration, Methodology, Funding acquisition, Data curation. **Nailiang Zhuang:** Writing – review & editing, Resources, Methodology, Formal analysis. **Xiaobin Tang:** Writing – review & editing, Validation, Software.

## Declaration of competing interest

The authors declare that they have no known competing financial interests or personal relationships that could have appeared to influence the work reported in this paper.

## Data availability

Data will be made available on request.

## Acknowledgements

This research is jointly supported by the National Natural Science Foundation of China (Grant No. 12205152), the Natural Science Foundation of Jiangsu Province (Grant No. BK20220904), the Fundamental Research Funds for the Central Universities (Grant No. NS2021060 and Grant No. NJ2022019-1).

## References

[1] Y. Song, N. Zhuang, H. Zhao, C. Ji, H. Deng, X. Tang, Conceptual design of a dual drum-controlled space molten salt reactor (D2-SMSR): Neutron physics and thermal hydraulics, Nucl. Eng. Technol. 55 (2023) 2315–2324.
[2] C. Yang, N. Zhuang, H. Zhao, X. Tang, Dynamic performance of the combined stirling thermoelectric conversion technology for a lunar surface nuclear power system, Appl. Therm. Eng. 221 (2023).
[3] H.-t. Liao, Overview of nuclear thermal propulsion technologies, Journal of Rocket Propulsion 37 (2011) 1–11.
[4] W. Emrich, Principles of Nuclear Rocket Propulsion, Elsevier, Oxford, 2016.
[5] Z. Vadim, P. Vladimir, Russian nuclear rocket engine design for mars exploration, Tsinghua Sci. Technol. 12 (2007) 256–260.
[6] M.E.M. Stewart, 3D reacting flow analysis of LANTR nozzles, AIP Conf. Proc. (2006) 858–869.
[7] T. Zhang, T. Jing, F. Qin, X. Sun, W. Li, G. He, Topology optimization of regenerative cooling channel in non-uniform thermal environment of hypersonic engine, Appl. Therm. Eng. 219 (2023).
[8] H. Wang, A. Zuo, H. Huo, X. Ma, System design selection and Parametric optimization analysis of 110kN nuclear thermal rocket engine, Atomic Energy Sci. Technol. 53 (2019) 30–38.
[9] Z. Li, H. Wang, Z. Cai, X. Ma, H. Sun, Numerical analysis of flow and heat transfer characteristics of 100 ton nuclear thermal rocket engine nozzle, Manned Spaceflight 24 (2018) 772–776.
[10] Z. Li, K. Xu, CFD simulation of non-equilibrium flow and heat transfer in thrust chamber of a 110 kN nuclear heat engine, Manned Spaceflight 26 (2020) 618–624.
[11] N.C. Salamon, Analysis of Nuclear Thermal Rocket Engine Coolant Channel Designs Enabled by Additive Manufacturing, The Ohio State University, 2020.
[12] W. Mullin, K. Melendez, B. Stefanko, A. Bell, G. Davis, E. Adu, J. Horack. Evaluating Regenerative Cooling Channels for Nuclear Thermal Propulsion with Additive Manufacturing, AIAA SciTech Forum, San Diego, 2022.
[13] Y. Li, F. Sun, G. Xie, J. Qin, Improved thermal performance of cooling channels with truncated ribs for a scramjet combustor fueled by endothermic hydrocarbon, Appl. Therm. Eng. 142 (2018) 695–708.
[14] Y. Chen, Y.T. Chew, B.C. Khoo, Heat transfer and flow structure in turbulent channel flow over protrusions, Int. J. Heat Mass Tran. 66 (2013) 177–191.
[15] H. Elmouazen, X. Zhang, M. Gibreel, M. Ali, Heat transfer enhancement of hydrogen rocket engine chamber wall by using V-shape rib, Int. J. Hydrogen Energy 47 (2022) 9775–9790.
[16] A.R. Shanmugam, K. Sun Park, Flow and heat transfer of supercritical hydrogen in a regenerative cooling channel with the arc ribs of a rocket engine, Appl. Therm. Eng. 236 (2024).
[17] M. Pizzarelli, F. Nasuti, M. Onofri, Trade-off analysis of high-aspect-ratio-cooling-channels for rocket engines, Int. J. Heat Fluid Flow 44 (2013) 458–467.
[18] J. Song, Y. Yuan, J. Liu, S. Luo, B. Sunden, Heat transfer enhancement of regenerative cooling Channel with pyramid lattice sandwich structures, Heat Tran. Eng. (2022) 1–15.
[19] P. Xie, X. Zhang, A method of rib-bed plate enhancing heat transfer in hydrogen rocket engine chamber wall, Int. J. Hydrogen Energy 44 (2019) 20504–20515.
[20] Y. Zhu, B. Liu, P. Jiang, Experimental and numerical investigations on n-decane thermal cracking at supercritical pressures in a vertical tube, Energy & fuels 28 (2014) 466–474.
[21] R.C. Hendricks, R.W. Graham, Y.Y. Hsu, R. Friedman, Experimental heat-transfer results for cryogenic hydrogen flowing in tubes at subcritical and supercritical pressures to 800 pounds per square inch absolute. National Aeronautics and Space Administration, 1966. NASA TN D-3095.